

The unchanging circumgalactic medium over the past 11 billion years

Hsiao-Wen Chen[⋆]

Department of Astronomy & Astrophysics, Kavli Institute for Cosmological Physics, University of Chicago, Chicago IL 60637, USA

Accepted 2012 September 4. Received 2012 August 27; in original form 2012 June 21

ABSTRACT

This paper examines how the circumgalactic medium (CGM) evolves as a function of time by comparing results from different absorption-line surveys that have been conducted in the vicinities of galaxies at different redshifts. Despite very different star formation properties of the galaxies considered in these separate studies and different intergalactic radiation fields at redshifts between $z \approx 2.2$ and $z \sim 0$, I show that both the spatial extent and mean absorption equivalent width of the CGM around galaxies of comparable mass have changed little over this cosmic time interval.

Key words: surveys – galaxies: haloes – quasars: absorption lines – galaxies: star formation.

1 INTRODUCTION

It is understood that galaxy growth is regulated by three competing processes: mergers, gas accretion that supplies the fuel necessary to support star formation, and feedback that returns gas and heavy elements to intergalactic space and consequently disrupts continuing gas accretion (Ceverino & Klypin 2009). Which process dominates and over what period of time determines not only the properties of the general galaxy population in different epochs, but also the chemical enrichment history of the intergalactic medium (IGM). Circumgalactic space provides a critical laboratory for investigating the interplay between star-forming regions and the IGM.

A powerful means to study and characterize the circumgalactic medium (CGM) is to carry out absorption spectroscopy of background quasi-stellar objects (QSOs) in the vicinities of distant galaxies. By searching for absorption features in the spectrum of the background QSO that are coincident in redshift with known galaxies in the foreground, empirical constraints on the CGM such as absorber strength and gas kinematics can be obtained at the projected separations between the galaxy and QSO pairs (e.g. Lanzetta et al. 1995; Bowen, Blades & Pettini 1995; Steidel et al. 2002). Unlike 21 cm observations which offer detailed two-dimensional maps of extended H I gas around individual galaxies, each QSO sightline provides only one measurement per galaxy. However, observations of a large sample of QSO–galaxy pairs with different projected separations can give a two-dimensional map of the CGM averaged over the entire galaxy sample.

Significant progress has been made over the past decade in mapping the CGM out to \sim 300 kpc projected distances at redshift $z\lesssim$ 0.5 using a large sample of QSO-galaxy pairs. This includes the spatial distributions of tenuous gas probed by the H_I Ly α 1215 absorption transition (e.g. Chen et al. 1998, 2001a; Tripp, Lu &

*E-mail: hchen@oddjob.uchicago.edu

Savage 1998; Prochaska et al. 2011), chemically enriched cool ($T \sim$ 10^4 K) clouds probed by the Mg II $\lambda\lambda$ 2796, 2803 absorption doublet (e.g. Chen & Tinker 2008; Kacprzak et al. 2008; Barton & Cooke 2009; Chen et al. 2010a,b; Gauthier, Chen & Tinker 2010; Gauthier & Chen 2011), chemically enriched ionized gas probed by the C_{IV} λλ 1548, 1550 absorption doublet (e.g. Chen, Lanzetta & Webb 2001b), and highly ionized warm gas probed by the O vi λλ 1031, 1037 absorption doublet (e.g. Chen & Mulchaey 2009; Prochaska et al. 2011; Tumlinson et al. 2011). However, studies of the CGM using QSO absorption spectroscopy become significantly more difficult with increasing redshift, both because the surface density of bright QSOs is low and because high-redshift galaxies are faint (for example, an L^* galaxy has $\mathcal{R} \approx 24.5$ mag at $z \sim 3$; see e.g. Adelberger & Steidel 2000) and moderate-resolution spectroscopy of these faint galaxies requires a large amount of telescope resources (e.g. Erb et al. 2003; Steidel et al. 2004; Simcoe et al. 2006).

At the same time, deep galaxy surveys like the Keck Baryonic Structure Survey (Steidel et al. 2004), the redshift survey in the Cosmological Evolution Survey (zCOSMOS; Lilly et al. 2007) and Deep Extragalactic Evolutionary Probe 2 (DEEP2; Newman et al. 2012) have yielded a large sample of spectroscopically identified galaxies z = 1-3. With a higher surface density, galaxies identified in the background in these surveys in principle provide an efficient means of densely mapping the CGM of foreground galaxies identified in the same surveys (e.g. Adelberger et al. 2005). The caveat is, however, that galaxies are faint and individual galaxy spectra do not provide a sufficient signal-to-noise ratio (S/N) for identifying weak absorption features in the foreground. Therefore, it is necessary to average together a large number of galaxy spectra in order to obtain sensitive constraints on the CGM at these high redshifts (e.g. Steidel et al. 2010; Bordoloi et al. 2011). While using galaxy-galaxy pairs has substantially improved the efficiency of probing the CGM using absorption spectroscopy, it is worth noting that absorption constraints derived from stacked spectra only give the mean properties of the gas averaged over a sample of galaxies and do not constrain the incidence or covering fraction of the gas.

With different empirical studies now available in the literature to characterize the CGM in different epochs, it is interesting to examine how the properties of the CGM have evolved with time. Both galaxies and the IGM exhibit very different properties at different redshifts. For example, most galaxies at z = 2-3 are seen actively forming stars at higher rates than most galaxies at low redshift z <0.5 (e.g. Ouchi et al. 2009). In addition, the ultraviolet background radiation field is more than 10 times higher at $z \approx 3$ than at $z \approx 0$ (e.g. Haardt & Madau 2012). Observations of the CGM as a function of redshift may provide key insights into the physical processes that drive the gas dynamics and chemical enrichment in circumgalactic space. This paper addresses the redshift evolution of the CGM by comparing different absorption-line studies of halo gas conducted at different redshifts. Despite very different star formation properties of the galaxies and different intergalactic radiation fields at redshifts from $z \approx 2.2$ to $z \sim 0$, I show that the extent and absorption strength of the CGM have not changed over the past 11 billion years. A Λ cosmology, $\Omega_{\rm M}=0.3$ and $\Omega_{\Lambda}=0.7$, with a Hubble constant $H_0=$ $70 \,\mathrm{km} \,\mathrm{s}^{-1} \,\mathrm{Mpc}^{-1}$ is adopted throughout the paper.

2 THE GALAXY SAMPLES

Five galaxy samples have been collected from the literature for studying the CGM across cosmic time. The galaxies are selected to have available constraints on the properties of their halo gas from absorption-line studies. In addition, the discussion focuses on the absorption species, H I, C IV and Mg II for which measurements are available from multiple epochs. A brief description of the galaxy samples and associated absorption-line measurements follows.

2.1 The Chen et al. (1998, 2001a,b) sample at $\langle z \rangle = 0.36$

Chen et al. (1998, 2001a) presented a sample of 47 galaxies at projected distances of $\rho \leq 300 \text{ kpc}^1$ (proper) from the lines of sight towards background QSOs and obtained measurements (or upper limits) of the associated Ly α absorption strength for individual galaxies in the spectra of the background QSOs. The galaxies in this sample span a broad range in rest-frame B-band luminosities (from $\approx 0.03 L_B^*$ to $\approx 3 L_B^*$ with a median of $\langle L_B \rangle = 0.6 L_B^*$), a broad range in redshifts (from z = 0.0752 to 0.8920 with a median of $\langle z \rangle = 0.3567$), and a range in impact parameter separations (from $\rho = 18$ to 250 kpc with a median of $\rho = 89$ kpc). High spatial resolution optical images obtained from the Hubble Space Telescope were available for classifying the morphological types of these galaxies according to the disc-to-bulge ratio (D/B) derived from a two-dimensional surface brightness profile analysis. The galaxies were found to exhibit a broad range of optical morphologies, including bulge-dominated elliptical/S0 (D/B < 3), earl-type spiral galaxies (3 < D/B < 14), late-type discs (D/B > 14) and galaxies with disturbed profiles that cannot be characterized by a normal disc or bulge.

To constrain the incidence and strength of tenuous gas around the 47 galaxies, Chen et al. (1998, 2001a) searched for the associated Ly α absorbers in the spectra of the background QSOs. They detected corresponding Ly α absorbers at velocity separations $|\Delta v| \leq 250 \,\mathrm{km \, s^{-1}}$ from 34 galaxies and placed 3σ upper limits to the rest-frame Ly α absorption equivalent width $W_r(1215)$ for the remaining 13 galaxies. The distribution of $W_r(1215)$ versus ρ for

this galaxy sample is shown in Fig. 1 (solid circles). These authors report a strong $W_r(1215)$ versus ρ anti-correlation (left-hand panel of Fig. 1; see also Lanzetta et al. 1995) that depends strongly on galaxy B-band luminosity, but not on galaxy morphology, mean surface brightness or redshift.

Using a likelihood analysis formulated to minimize the scatter in the $W_r(1215)$ versus ρ anti-correlation, Chen et al. (1998, 2001a) concluded that the extent of tenuous gas around galaxies scales with galaxy B-band luminosity as $R_{\rm Ly\alpha}/R_{\rm Ly\alpha}^* = (L_B/L_B^*)^{0.39\pm0.09}$ where $R_{\rm Ly\alpha}^* \approx 300$ kpc for $W_r(1215) = 0.3$ Å (right-hand panel of Fig. 1) and that the mean gas covering fraction is \gtrsim 86 per cent within $\rho = R_{\rm Ly\alpha}$. The improved $W_r(1215)$ versus ρ anti-correlation after taking into account the luminosity normalization of the projected distances strongly supports that the absorbers trace tenuous gas in individual haloes surrounding the galaxies rather than tenuous gas in galaxy groups or large-scale filaments around the galaxy overdensities.

In a follow-up paper, Chen et al. (2001b) examined the incidence and strength of C IV absorption features in the vicinities of 50 galaxies. They detected C IV absorption features at velocity separations $|\Delta v| \leq 250 \,\mathrm{km \, s^{-1}}$ from 14 galaxies and placed 3σ upper limits to the rest-frame C IV λ 1548 absorption equivalent width W_r (1548) for the remaining 36 objects. These authors found that while the W_r (1548) versus ρ distribution exhibits a large scatter, there appears to a distinct boundary between C IV-absorbing and non-absorbing regions in galactic haloes. Based on a likelihood analysis formulated to minimize the scatter between detections and non-detections in the W_r (1548) versus ρ distribution, Chen et al. concluded that the extent of C IV-enriched gas scales with galaxy B-band luminosity as $R_{\rm C IV}/R_{\rm C IV}^* = (L_B/L_B^*)^{0.5\pm0.1}$ where $R_{\rm C IV}^* \approx 160 \,\mathrm{kpc}$. The luminosity-normalized W_r (1548) versus ρ distribution is presented in Fig. 2 (solid circles).

Fig. 2 shows that while the mean covering fraction of C Ivenriched gas within $\rho=R_{\rm C\,IV}$ is high, $\gtrsim 90$ per cent, around these low-redshift galaxies, the scatter in the $W_r(1548)$ versus ρ relation is also large. To facilitate a comparison between different studies, the galaxies within 160 kpc of the QSO sightlines in the low-redshift study are divided into subsamples according to the impact parameter bins adopted by Steidel et al. (2010). The 1σ clipped mean and dispersion of $W_r(1548)$ in each subsample of Chen et al. (2001b) are shown as the pentagon symbols and the associated error bars.

Note that with a large scatter in $W_r(1548)$, the strongest absorbers naturally dominate in calculating the mean value over a small sample of approximately five galaxies per impact parameter bin (cf. ~ 100 galaxies per impact parameter bin in the stacks of Steidel et al.). Applying a 1σ clipping criterion allows a more accurate assessment of the mean intrinsic properties based on a rough estimate of the underlying $W_r(1548)$ distribution. As a result of the clipping criterion, one galaxy at luminosity-normalized $\rho > 100\,\mathrm{kpc}$ with an associated C IV absorber of $W_r(1548) \approx 1.7\,\mathrm{\mathring{A}}$ is found to fall outside of the 1σ range and excluded from the mean calculation. This is the only galaxy excluded in the 1σ clipped mean calculation of the Chen et al. sample.

2.2 The Chen et al. (2010a) sample at $\langle z \rangle = 0.25$

Using a sample of 94 galaxies spectroscopically identified at redshifts between z=0.11 and z=0.49 with a median redshift of $\langle z \rangle = 0.24$ and located at $\rho \lesssim 170\,\mathrm{kpc}$ from the line of sight of a background QSO, Chen et al. (2010a) examined the incidence and

 $^{^1}$ All numbers quoted in this paper have been corrected for the standard Λ cosmology.

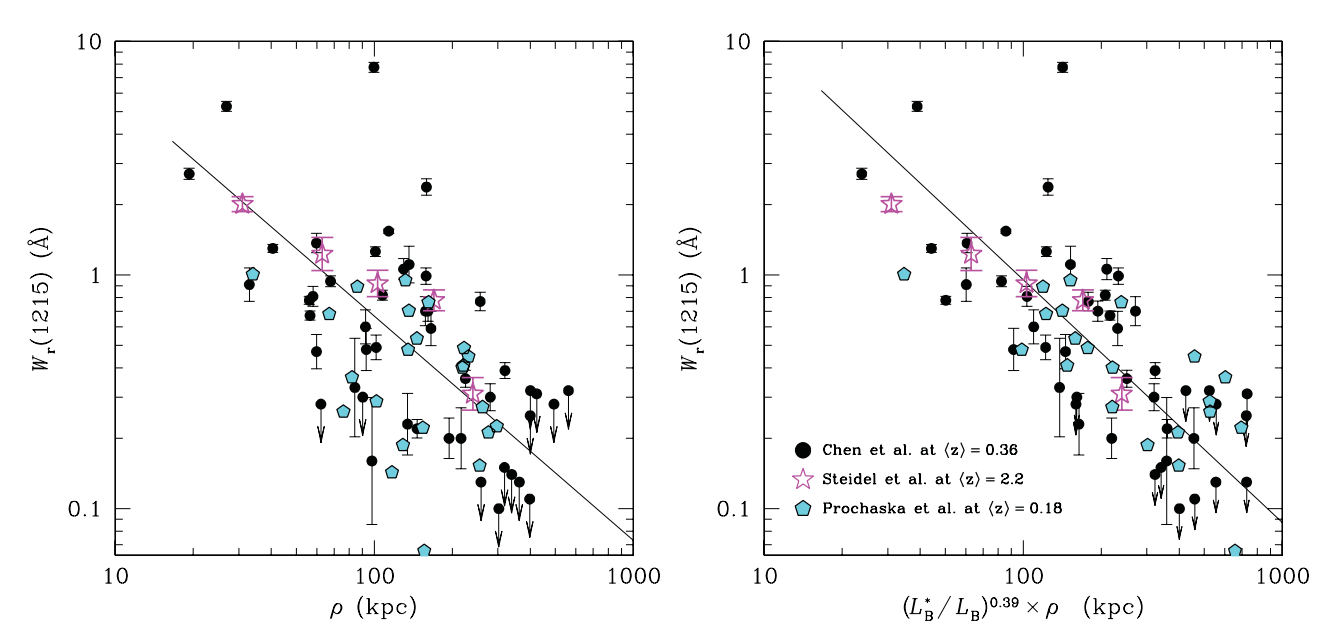


Figure 1. Observed incidence and strength of Ly α absorbers in the vicinities of galaxies over the redshift range from $z \sim 0$ to $z \sim 2.5$. The left-hand panel shows the rest-frame Ly α absorption equivalent width $W_r(1215)$ versus the projected distance of the absorbing galaxy ρ in physical coordinates. Solid circles are galaxies from Chen et al. (1998, 2001a) with a median redshift of $\langle z \rangle = 0.36$. Pentagons are galaxies from Prochaska et al. (2011) with a median redshift of the absorber strength, while points with arrows indicate 3σ upper limits for non-detections. The solid line represents the power-law model of Chen et al. (2001a) that best characterizes the observed $W_r(1215)$ versus ρ inverse correlation for the $\langle z \rangle = 0.36$ sample. The right-hand panel shows the rest-frame Ly α absorption equivalent width $W_r(1215)$ versus projected distance normalized by B-band luminosity (L_B) for the low-redshift galaxy samples of Chen et al. and Prochaska et al. The luminosity scaling relation is adopted from Chen et al. for the $\langle z \rangle = 0.36$ sample. The best-fitting power-law function (solid line) was determined based on a likelihood analysis that minimizes the scatter in the $W_r(1215)$ versus ρ relation. The high-redshift measurements from Steidel et al. (star symbols) were made based on stacks of ~ 100 galaxies with a mean luminosity of roughly L^* (D. Erb, private communication; see also Steidel et al. 2004). Therefore, no scaling has been applied to these measurements in the right-hand panel (star symbols).

strength of Mg II absorption features around galaxies. The galaxies in this sample span a broad range in rest-frame B-band luminosities, from $\approx 0.04~L_B^*$ to $\approx 4~L_B^*$ with a median of $\langle L_B \rangle = 0.8~L_B^*$, and a broad range in rest-frame $B_{AB} - R_{AB}$ colours from $B_{AB} - R_{AB} \approx 0$ to $B_{AB} - R_{AB} \approx 1.5$. In a follow-up study, Chen et al. (2010b) estimated the total stellar mass and mean star formation rate average over the last 10 Myr by analysing the broad-band spectral energy distribution of these galaxies. The galaxies are found to span a stellar mass range from $\log M_{\rm star} = 8.5$ to $\log M_{\rm star} = 11.6$ with a median of $\langle \log M_{\rm star} \rangle = 10.3$ and a range in specific star formation rate from \log sSFR = -11.7 to \log sSFR = -8.7 with a median of $\langle \log$ sSFR $\rangle = -10.1$.

Excluding galaxies with known neighbours at $\rho < 200\,\mathrm{kpc}$, Chen et al. (2010a) detected corresponding Mg II absorbers at velocity separations $|\Delta\,v|\lesssim 300\,\mathrm{km\,s^{-1}}$ 47 galaxies and placed 2σ upper limits to the rest-frame Mg II λ 2796 absorption equivalent width $W_r(2796)$ for the remaining 24 galaxies. Similar to the study of extended Ly α absorbing gas, these authors report a strong $W_r(2796)$ versus ρ anti-correlation that depends strongly on galaxy *B*-band luminosity or stellar mass, but not on galaxy colours or redshift (Chen et al. 2010a,b). Based on a likelihood analysis formulated to minimize the scatter in the $W_r(2796)$ versus ρ anti-correlation, the authors concluded that the extent of Mg II-enriched gas around galaxies scales with galaxy *B*-band luminosity as $R_{\mathrm{Mg\,II}}/R_{\mathrm{Mg\,II}}^* = (L_B/L_B^*)^{0.35\pm0.03}$ where $R_{\mathrm{Mg\,II}}^* \approx 107\,\mathrm{kpc}$ and that the mean gas covering fraction is ≈ 80 per cent within $\rho = R_{\mathrm{Mg\,II}}$ for absorbers of $W_r(2796) \geq 0.1\,\mathrm{\mathring{A}}$.

The luminosity-normalized $W_r(2796)$ versus ρ distribution is presented in Fig. 3 (solid circles). Outliers identified based on a 3σ

clipping criterion are highlight in dotted circles. Galaxies with close neighbours are indicated by open symbols.

2.3 The Steidel et al. (2010) sample at $\langle z \rangle = 2.2$

Steidel et al. (2010) examined the CGM at z > 2 using a sample of 512 close galaxy pairs separated by \lesssim 15 arcsec. At the median redshift of the galaxy pair sample $\langle z \rangle = 2.2$, an angular separation of 15 arcsec corresponds to projected separations of \$\leq\$124 kpc. Galaxies in each pair are found at cosmologically distinct redshifts with line-of-sight velocity separation $> 3000 \,\mathrm{km \, s^{-1}}$, and therefore the background galaxy serves as a random probe of unseen gas associated with the foreground galaxy (see also Adelberger et al. 2005). R-band magnitudes of these galaxies range from $\mathcal{R}=22$ to $\mathcal{R}=25.5$ with a median $\langle \mathcal{R} \rangle \approx 24.3$ (e.g. Steidel et al. 2004), corresponding to roughly L^* at $z \sim 2.3$ (e.g. Reddy & Steidel 2009). The mean stellar mass of these galaxies is found to be around $\langle \log M_{\rm star} \rangle \approx 10.3$ (Shapley et al. 2005). Many of these galaxies are actively forming stars, showing relatively luminous UV fluxes and strong blueshifted self-absorption in the UV ISM lines (e.g. Shapley et al. 2003; Steidel et al. 2004; Adelberger et al. 2005).

To map the CGM of these star-forming galaxies, Steidel et al. first divided the galaxy sample in three impact parameter bins, $\rho \le 41$ kpc, $\rho = 41 - 83$ kpc and $\rho = 83 - 124$ kpc, and in each bin they formed an average spectrum of the background galaxies after shifting the individual spectra to the rest frame of their foreground members. The mean spectra were of high S/N and revealed several absorption features imprinted by the CGM of the foreground galaxies. These include hydrogen Ly α λ 1215, C IV $\lambda\lambda$ 1548, 1550

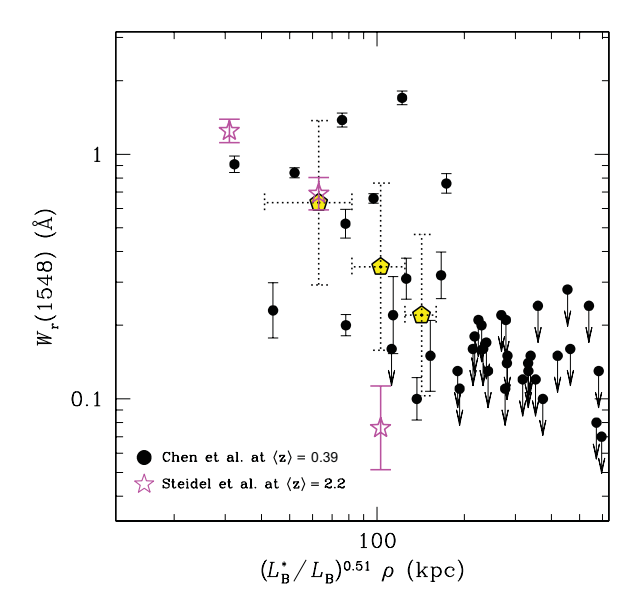


Figure 2. Observed incidence and strength of C IV absorbers in the vicinities of galaxies from two different redshift ranges, $z \lesssim 0.5$ and $z \sim 2.5$. Solid circles are galaxies from Chen et al. (2001b) with a median redshift of $\langle z \rangle = 0.39$. Error bars indicate the 1σ measurement uncertainties of the absorber strength, while points with arrows indicate 3σ upper limits for non-detections. Impact parameters of these galaxies have been normalized by their B-band luminosity according to the best-fitting scaling relation of Chen et al. (2001b) that minimizes the scatter between detections and nondetections. Star symbols are galaxies from Steidel et al. (2010) with a median redshift of $\langle z \rangle = 2.2$ and a mean luminosity of roughly L^* . Because the absorption spectra of Steidel et al. did not have sufficient resolution to resolve the C_{IV} doublet, these authors reported the combined absorption equivalent width of the doublets. The star symbols and associated error bars in this panel indicate the estimated absorption strength of the C IV λ 1548 component and its associated uncertainties due to measurement errors and uncertain doublet ratios (in cases of saturated lines). To facilitate the comparison between lowand high-redshift samples, the galaxies within 160 kpc of the QSO sightlines in the low-redshift study are divided into subsamples according to the impact parameter bins adopted by Steidel et al. (2010). The 1σ clipped mean and dispersion of $W_r(1548)$ in each subsample of Chen et al. (2001b) are shown as the pentagon symbols and the associated error bars.

and Si II λ 1260, although the relatively low resolution of the spectra did not allow the authors to resolve the C IV doublet.

Measurements of the absorber strength versus impact separation from Steidel et al. (2010) are included in Figs 1 through 3 (star symbols) for direct comparisons with observations of the CGM at lower redshifts. Note that the $W_r(1215)$ measurements at $\rho > 125 \,\mathrm{kpc}$ were made using stacks of high S/N spectra of background QSOs in the rest frame of 21 foreground galaxies. In addition, the original C_{IV} absorption strength reported by Steidel et al. (2010) include both components of the doublet. The values and associated uncertainties of $W_r(1549)$ for the $z \approx 2.2$ galaxies in Fig. 2 are estimated based on a range of possible C IV doublet ratio from 2:1 to 1:1 due to line saturation. Finally, Mg II absorption doublets are redshifted into the near-infrared spectral window at $z \gtrsim 2.2$, and are therefore missed in the available optical spectra of Steidel et al. (2010). However, the Si⁺ and Mg⁺ ions have comparable ionization potentials and are observed to coexist in a broad range of astrophysical environment (e.g. Sembach & Savage 1996; Churchill et al. 2000; Ganguly et al. 2005). It is therefore justified to infer the associated Mg II absorption strength $W_r(2796)$ of the $z \approx 2.2$ galaxies based on known absorption strength of Si II λ 1260, W_r (1260) from Steidel et al. Based on the observations of Churchill et al. (2000), I estimate

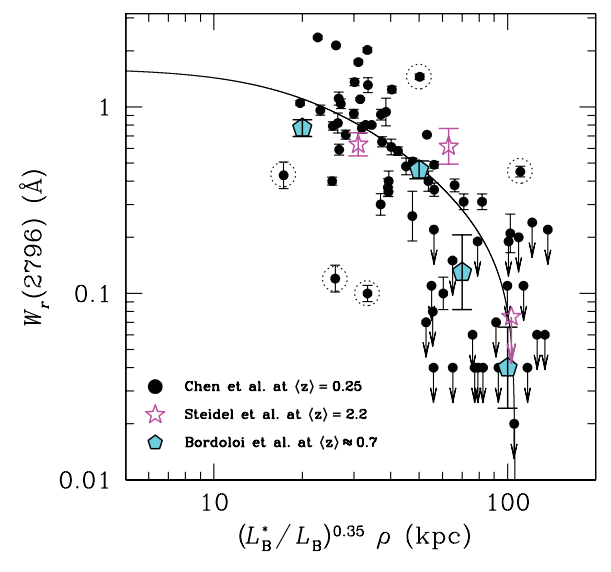


Figure 3. Observed incidence and strength of Mg II absorbers in the vicinities of galaxies from three different epochs, $z \le 0.5$, z = 0.5-0.9 and $z \sim 2.5$. Solid circles are galaxies from Chen et al. (2010a) with a median redshift of $\langle z \rangle = 0.24$. Error bars indicate the 1σ measurement uncertainties of the absorber strength, while points with arrows indicate 2σ upper limits for nondetections. Impact parameters of these galaxies have been normalized by their B-band luminosity according to the best-fitting scaling relation of Chen et al. (2010a) from a likelihood analysis that strengthens the $W_r(2796)$ versus ρ inverse correlation. The likelihood analysis excluded outliers (points with dotted circles) identified using a 3σ clipping criterion. The solid curve represents the best-fitting model that follows a r^{-2} density profile of maximum extent $R_{\text{Mg II}}$ (see Chen et al. 2010a for details). Pentagons are for blue galaxies at z = 0.5–0.9 from Bordoloi et al. (2011) with $I_{AB} \le 22.5$ and a median redshift of $\langle z \rangle \approx 0.7$. At z = 0.7, $I_{AB} = 22.5$ corresponds to L^* . Therefore, the measurements of Bordoloi et al. have not been corrected for luminosity differences. Star symbols are the expected $W_r(2796)$ for $\sim L_*$ galaxies at $\langle z \rangle = 2.2$, based on the rest-frame absorption equivalent width of the Si II λ 1260 transition $W_r(1260)$ from Steidel et al. (2010). At $z \gtrsim 1$ 2.2, Mg II absorption doublets are redshifted into the near-infrared spectral window and not observed by optical spectra. The expected $W_r(2796)$ is calculated based on the empirical correlation, $W_r(2796) \approx 1.5 W_r(1260)$, extracted from observations of Churchill et al. (2000).

that $W_r(2796) \approx 1.5 W_r(1260)$. The inferred $W_r(2796)$ of the $z \approx 2.2$ galaxies are shown in Fig. 3 as star symbols.

2.4 The Prochaska et al. (2011) sample at $\langle z \rangle = 0.18$

Prochaska et al. (2011) conducted a galaxy survey in the fields of 14 QSOs at $z_{\rm QSO}=0.06$ –0.57 for which UV absorption spectra were available for searching Ly α and O vI absorption features associated with the low-redshift CGM. The survey reached >60 per cent completeness for galaxies brighter than R=19.5 mag within 5 arcmin radius of the QSO lines of sight. The galaxies in this sample span a broad range in rest-frame B-band luminosities, from ≈ 0.01 L_B^* to ≈ 5 L_B^* with a median of $\langle L_B \rangle = 0.3$ L_B^* , and a broad range in redshifts, from z=0.005 to 0.5 with a median of $\langle z \rangle = 0.18$.

Considering only galaxies at $\rho \leq 300$ kpc from the lines of sight towards background QSOs, the authors examined the incidence and strength of Ly α in the vicinities of these galaxies. Crosses in Fig. 1 represent the results from Prochaska et al. (2011) with (right-hand panel) and without (left-hand panel) the luminosity scaling.

2.5 The Bordoloi et al. (2011) sample at $\langle z \rangle \approx 0.7$

The zCOSMOS team (Lilly et al. 2007) has produced a large sample of spectroscopically identified galaxies with $I_{\rm AB} \leq 22.5$ mag at z=0–1.4 over the $2 \deg^2$ sky area covered by the COSMOS project (Scoville et al. 2007). Additional spectroscopic data have also been obtained in the follow-up zCOSMOS-deep effort that targeted fainter galaxies (B < 25.5 mag) in the inner $1 \deg^2$ region of the COSMOS field with photometric redshifts $z_{\rm phot} > 1$. Taking advantage of the existing large galaxy survey data, Bordoloi et al. (2011) adopted the approach of Steidel et al. (2010) and examined the properties of the metal-enriched CGM at intermediate redshifts based on the incidence and strength of Mg II absorbers in the vicinities of zCOSMOS galaxies.

Specifically, Bordoloi et al. first identified foreground galaxies with redshift accurately known at z = 0.5-0.9 from the zCOSMOSbright sample. These authors then identified background galaxies with spectra available from zCOSMOS-deep. Although the zCOSMOS-deep spectra did not have sufficient quality for measuring the redshifts for some of these objects, the $z_{\text{phot}} > 1$ selection criterion ensures that the majority of these objects are at z > 1and therefore their optical spectra are still useful for searching for intervening absorption features at z < 1. Cross-correlating the two galaxy samples, Bordoloi et al. identified a sample of \approx 3900 galaxies at z = 0.5–0.9 and located within $\rho \le 200$ kpc of a background galaxy. The spectra of the background galaxies were co-added in the rest frame of the foreground objects. The spectral coverage allowed these authors to search for Mg II absorption features associated with the foreground galaxies and to examine the properties of the metal-enriched CGM based on the observed spatial distribution of $W_r(2796)$. The observed $W_r(2796)$ versus ρ distribution for blue galaxies from Bordoloi et al. (2011) is shown as cyan crosses in Fig. 3.

Note that the consideration of only blue galaxies from Bordoloi et al. is justified here by their mean stellar mass range $\langle \log M_{\rm star} \rangle = 10$ –10.3, which is comparable to galaxies in the Chen et al. sample (Section 2.2) and Steidel et al. (Section 2.3) samples shown in the same figure. The red galaxies in the Bordoloi et al. sample are more massive with $\langle \log M_{\rm star} \rangle \approx 10.7$. In addition, Chen et al. (2010b) showed that the majority of galaxies in the Chen et al. (2010a) sample fall on the blue sequence. Few galaxies exhibit colours that are consistent with red galaxies in the field. Most of their red galaxies also turned out to be in a group environment and were excluded from their analysis. The incidence and strength of Mg II absorbers around massive red galaxies have been found suppressed relative to younger and lower mass objects (e.g. Gauthier et al. 2010; Bordoloi et al. 2011; Gauthier & Chen 2011). The red sample of Bordoloi et al. is therefore not considered in this study.

Finally, the exact distribution of *B*-band luminosity in Bordoloi et al. sample is not known. However, at z=0.7, the limiting magnitude $I_{\rm AB}=22.5$ of the zCOSMOS sample corresponds to L^* (see e.g. Faber et al. 2007). Therefore the measurements of Bordoloi et al. have not been corrected for luminosity differences in Fig. 3.

3 DISCUSSION

The collection of five absorption-line surveys in the vicinities of distant galaxies offers a unique opportunity to examine for the first time how the properties of the CGM have evolved with redshift. It is immediately clear from Figs 1–3 that the observed absorber strength versus luminosity-normalized projected distance does not vary from $z \approx 2.2$ to $z \sim 0$ for ionized gas probed by either hydrogen,

Table 1. Summary of the galaxy samples for CGM studies.

Sample	Probe	$\langle z \rangle$	χ^2 test
	Hydrogen absorption		
Chen et al. (1998, 2001a)	QSO-galaxy	0.36	
Steidel et al. (2010)	Galaxy–galaxy	2.20	99 per cent
Prochaska et al. (2011)	QSO–galaxy	0.18	99 per cent
	C IV absorption		
Chen et al. (2001b)	QSO-galaxy	0.39	
Steidel et al. (2010)	Galaxy–galaxy	2.20	80 per cent
	Mg II absorption		
Chen et al. (2010a)	QSO-galaxy	0.25	
Steidel et al. $(2010)^a$	Galaxy–galaxy	2.20	97 per cent
Bordoloi et al. (2011)	Galaxy–galaxy	≈0.7	99 per cent

 $[^]a$ As described in the text, the Mg II absorption strength here is inferred from the reported Si II 1260 transition.

C IV, or Mg II transitions. To assess the statistical significance of the observed lack of redshift evolution, I perform a χ^2 test to compare the absorption properties of the CGM at different redshifts. The results are summarized in Table 1.

Specifically, I first adopt the best-fitting power-law function of Chen et al. (2001a) at $\langle z \rangle = 0.36$ as the fiducial model. Then I estimate the probability of the observed radial distribution of hydrogen absorption around $\langle z \rangle = 2.2$ galaxies being drawn from the fiducial model. I find that the probability of the two samples sharing the same parent distribution is >99 per cent. Next, I repeat the same approach for Mg II absorbing gas, adopting the best-fitting model profile of Chen et al. (2010a) at $\langle z \rangle = 0.25$ as the fiducial model and estimating the probability of each of the Bordoloi et al. (2011) and Steidel et al. (2010) samples being drawn from the fiducial model. I find that the probability of galaxies possessing the same radial absorption profile of low-ionization species since z = 2.2 is better than 97 per cent. The result for C IV absorbing gas is more uncertain, because fewer galaxies were found at luminosity-normalized ρ < 160 kpc in the low-redshift sample. Owing to the observed large scatter in Fig. 2, no analytic model presents a good fit to the data. The χ^2 test is therefore performed based on comparisons of the binned data (pentagons versus star symbols in Fig. 2). This exercise also yields a high probability of 80 per cent that the low- and high-redshift samples share similar C IV absorption properties in the CGM. In summary, the χ^2 test therefore supports the conclusion that the CGM exhibits little change in the absorption properties over the redshift range from z = 0.2 to z = 2.2.

Note that the lack of variation applies to both mean absorption equivalent width and the spatial extent of the CGM traced by either hydrogen or heavy ions such as C³+ and Mg⁺. The absorption features adopted for the comparison are all strong transitions and are likely saturated. Although measurements of the rest-frame absorption equivalent width for saturated lines do not constrain the underlying total gas column densities, they constrain the mean number of absorbing clumps and gas kinematics along the lines of sight (e.g. Petitjean & Bergeron 1990; Prochter, Prochaska & Burles 2006). It is therefore important to keep in mind that the agreement in the mean absorption equivalent width between the CGM at low and high redshifts reflects primarily similar kinematics and volume filling factor of gaseous clumps, not total gas density, in galactic haloes. But whether or not the absorption lines are saturated does not change the conclusion that the spatial extent (≈100 kpc) of the

chemically CGM has varied little with time. Here I consider possible systematics and implications.

3.1 Point sources versus extended background light

A fundamental difference between CGM studies at low and high redshifts is the use of point-like QSOs versus spatially extended galaxies as the background light source. The UV continuum emission regions of QSOs are <1 pc (e.g. Blackburne et al. 2012), while galaxies at z > 1 have a typical half-light radius of \sim 2–3 kpc (e.g. Law et al. 2007). If the foreground gaseous clouds do not fully cover the background galaxies, then the absorption equivalent width would appear to be weaker than what is seen in the spectrum of a background QSO when the QSO light is fully covered by the clouds. Comparisons between measurements made along QSO and galaxy sightlines therefore need to take into account the effect of possible partial covering fractions.

A key result in the low-redshift surveys summarized in Section 2 is that the covering fraction of extended gas around galaxies is nearly unity. Specifically, the mean covering fraction of tenuous gas probed by Ly\$\alpha\$ is \$\geq 86\$ per cent within \$\rho = R_{\text{Ly}\alpha}\$; the mean covering fraction of C iv-enriched gas within \$\rho = R_{\text{C iv}}\$ is \$\geq 90\$ per cent; and the mean covering fraction of Mg ii-enriched gas within \$\rho = R_{\text{Mg ii}}\$ is \$\geq 80\$ per cent. Accounting for possible partial covering fractions is therefore unlikely to change the measurements of Bordoloi et al. (2011) and Steidel et al. (2010) by more than 20 per cent. A high gas covering fraction is confirmed in CGM surveys at \$z \geq 1\$ using QSO probes by Lovegrove & Simcoe (2011) and by Adelberger et al. (2005), albeit with large uncertainties due to a small sample size.

3.2 Random velocity offsets between galaxies and absorbers

Random velocity offsets between absorbing gas and the systemic motion of the absorbing galaxy can in principle result in a suppressed absorption signal in stacked spectra (e.g. Ellison et al. 2000). If this is a dominant effect, then the measurements of Bordoloi et al. (2011) and Steidel et al. (2010) should be treated as lower limits.

The velocity separation between galaxies and absorbers identified along QSO lines of sight is well characterized by a Gaussian distribution function (e.g. Lanzetta, Webb & Barcons 1997; Chen et al. 2010a). Specifically, the velocity dispersion between Mg II absorbers and their absorbing galaxies is found to be $\sigma_{\rm v} \approx 137 \, {\rm km \, s^{-1}}$ (Chen et al. 2010a). To assess the magnitude of such systematic bias, I perform a Monte Carlo simulation that creates stacks of 50 to 100 individual mocked absorption spectra with a spectral resolution of fullwidthathalf-maximum $\approx 350 \, \mathrm{km \, s^{-1}}$ (comparable to the spectral quality for the high-redshift CGM studies) and varying S/N from 5 to 10. A synthetic absorption feature is randomly placed in each mocked spectrum following a Gaussian distribution function around a fiducial position. I experiment with different widths of the Gaussian distribution function, ranging from $\hat{\sigma}_v = 50$ to $\hat{\sigma}_{v} = 600 \,\mathrm{km}\,\mathrm{s}^{-1}$, and measure the absorption equivalent widths in the stacked spectra. The results of the Monte Carlo simulation study show that for 0.1-Å absorbers one can recover the full absorption equivalent width at $\hat{\sigma}_{\rm v} \lesssim 200\,{\rm km\,s^{-1}}$. At $\hat{\sigma}_{\rm v} \approx 300\,{\rm km\,s^{-1}}$, the absorption equivalent width may be underestimated by ≈ 20 per cent. Given that the velocity dispersion between galaxies and their absorbers is less than 200 km s⁻¹, I find it unlikely that the absorption equivalent width measurements in stacked spectra are significantly underestimated due to random velocity offsets between gas and galaxies.

3.3 The nature of L^* galaxies at different redshifts

The spatial profiles of the CGM absorption shown in Figs 1 through 3 are based on luminosity-normalized projected distances. This is motivated by the expectation that more massive galaxies possess more extended gas (e.g. Mo & Miralda-Escude 1996). Because the observations are calibrated with respect to L^* -type galaxies in different epochs, it is also necessary to examine the intrinsic properties of L^* galaxies at different redshifts before attempting to understand the lack of variation in the observed spatial distributions of absorbers around distant galaxies.

Using an abundance matching approach, several authors have estimated the mean halo mass for galaxies of different luminosity/mass at different epochs (e.g. Zheng, Coil & Zehavi 2007; Conroy et al. 2008). At low redshifts, L^* galaxies are found to reside on average in $M_{\rm h} \sim 10^{12}\,{\rm M}_{\odot}$ haloes based on a luminosity-dependent mapping between galaxies and dark matter haloes (Zheng et al. 2007). Likewise, Conroy et al. (2008) found that the majority of spectroscopically identified star-forming galaxies at $z\sim 2$ reside in haloes of $M_{\rm h} \sim 10^{12}\,{\rm M}_{\odot}$. Therefore, L^* galaxies appear to reside in haloes of comparable mass at these different redshifts.

This conclusion remains if one infers the mean halo mass of these galaxies based on the mean observed stellar masses. At both low and high redshifts, these galaxies are typically found to contain $M_{\rm star} \sim 2 \times 10^{10} \, {\rm M_{\odot}}$, which leads to a typical dark matter halo mass of $M_{\rm h} \sim 10^{12} \, {\rm M_{\odot}}$ (e.g. Conroy & Wechsler 2009; Behroozi, Conroy & Wechsler 2010; Moster et al. 2010). Together results of this exercise confirm that the comparisons shown in Figs 1 through 3, after the normalization to L^* galaxies, are for haloes of comparable mass and therefore support the conclusion that the spatial extent and mean absorption strength of the CGM in haloes of comparable mass have changed little since $z \sim 2$.

3.4 Implications

The consistent spatial profiles of different species in the CGM from $z\approx 2.2$ to $z\sim 0$ are difficult to interpret, whether the observed absorbers originate in starburst driven outflows (e.g. Martin & Bouché 2009; Weiner et al. 2009; Rubin et al. 2010) or in infalling clouds (e.g. Heitsch & Putman 2009). In particular, galaxies at z=2--3 are seen actively forming stars and super galactic winds may be effective in replenishing the CGM with metal-enriched gas (e.g. Murray, Ménard & Thompson 2011). In contrast, galaxies at z<0.5 are more quiescent with a diverse star formation history and super galactic winds are not expected to be the primary explanation for the high incidence and covering fraction of metal-enriched, cool halo gas out to $100\,\mathrm{kpc}$.

At the same time, the intergalactic ultraviolet radiation field has declined by more than a factor of 10 from z=2–3 to $z\sim0$. Cool clouds are expected to form at larger galactic distances at lower redshifts (e.g. Mo & Miralda-Escude 1996). If the observed absorbers originate in infalling cool clouds, then the spatial profile is expected to be more extended at lower redshift, which also disagrees with the trend shown in Section 2.

In summary, comparisons between different absorption-line surveys conducted in the vicinities of galaxies at different redshifts have revealed a puzzling finding. Despite very different star formation properties of the galaxies considered in these separate studies and different intergalactic radiation fields at redshifts between $z \approx 2.2$ and $z \sim 0$, the spatial extent and mean absorption strength of the CGM around galaxies of comparable mass appear to be unchanged over this cosmic time interval. The observed lack of variation in

1244 H.-Wen Chen

the CGM properties at different redshifts provides a critical test of theoretical models of gas flows around galaxies.

ACKNOWLEDGMENTS

It is a pleasure to thank Nick Gnedin, Sean Johnson, Andrey Kravtsov, Lynn Matthews and Michael Rauch for important discussions. I thank Sean Johnson, Lynn Matthews and Michael Rauch for helpful comments on an earlier version of this paper.

REFERENCES

Adelberger K. L., Steidel C. C., 2000, ApJ, 544, 218

Adelberger K. L., Shapley A. E., Steidel C. C., Pettini M., Erb D. K., Reddy N. A., 2005, ApJ, 629, 636

Barton E. J., Cooke J., 2009, AJ, 138, 1817

Behroozi P. S., Conroy C., Wechsler R. H., 2010, ApJ, 717, 379

Blackburne J. A., Kochanek C. S., Chen B., Dai X., Chartas G., 2012, ApJ, preprint (arXiv:1112.0027)

Bordoloi R. et al., 2011, ApJ, 743, 10

Bowen D. V., Blades J. C., Pettini M., 1995, ApJ, 448, 634

Ceverino D., Klypin A., 2009, ApJ, 695, 292

Chen H.-W., Mulchaey J. S., 2009, ApJ, 701, 1219

Chen H.-W., Tinker J. L., 2008, ApJ, 687, 745

Chen H.-W., Lanzetta K. M., Webb J. K., Barcons X., 1998, ApJ, 498, 77

Chen H.-W., Lanzetta K. M., Webb J. K., Barcons X., 2001a, ApJ, 559, 654

Chen H.-W., Lanzetta K. M., Webb J. K., 2001b, ApJ, 556, 158

Chen H.-W., Helsby J. E., Gauthier J. R., Shectman S. A., Thompson I. B., Tinker J. L., 2010a, ApJ, 714, 1521

Chen H.-W., Wild V., Tinker J. L., Gauthier J.-R., Helsby J. E., Shectman S. A., Thompson I. B., 2010b, ApJ, 724, L176

Churchill C. W., Mellon R. R., Charlton J. C., Jannuzi B. T., Kirhakos S., Steidel C. C., Schneider D. P., 2000, ApJS, 130, 91

Conroy C., Wechsler R. H., 2009, ApJ, 696, 620

Conroy C., Shapley A. E., Tinker J. L., Santos M. R., Lemson G., 2008, ApJ, 679, 1192

Ellison S. L., Songaila A., Schaye J., Pettini M., 2000, AJ, 120, 1175

Erb D. K., Shapley A. E., Steidel C. C., Pettini M., Adelberger K. L., Hunt M. P., Moorwood A. F. M., Cuby J.-G., 2003, ApJ, 591, 101

Faber S. M. et al., 2007, ApJ, 665, 265

Ganguly R., Sembach K. R., Tripp T. M., Savage B. D., 2005, ApJS, 157, 251

Gauthier J.-R., Chen H.-W., 2011, MNRAS, 418, 2730

Gauthier J.-R., Chen H.-W., Tinker J. L., 2010, ApJ, 716, 1263

Haardt F., Madau P., 2012, ApJ, 746, 125

Heitsch F., Putman M. E., 2009, ApJ, 698, 1485

Kacprzak G. G., Churchill C. W., Steidel C. C., Murphy M. T., 2008, AJ, 135, 922

Lanzetta K. M., Bowen D. V., Tytler D., Webb J. K., 1995, ApJ, 442, 538

Lanzetta K. M., Webb J. K., Barcons X., 1997, in Petitjean P., Charlot S., eds, Proc. 13th IAP Colloq., Structure and Evolution of the Intergalactic Medium from QSO Absorption Line Systems. Editions Frontières, Paris, p. 213

Law D. R., Steidel C. C., Erb D. K., Pettini M., Reddy N. A., Shapley A. E., Adelberger K. L., Simenc D. J., 2007, ApJ, 656, 1

Lilly S. J. et al., 2007, ApJS, 172, 70

Lovegrove E., Simcoe R. A., 2011, ApJ, 740, 30

Martin C. L., Bouché N., 2009, ApJ, 703, 1394

Mo H. J., Miralda-Escudé J., 1996, ApJ, 469, 589

Moster B. P., Somerville R. S., Maulbertsch C., van den Bosch F. C., Macciò A. V., Naab T., Oser L., 2010, ApJ, 710, 903

Murray N., Ménard B., Thompson T. A., 2011, ApJ, 735, 66

Newman J. et al., 2012, ApJS, preprint (arXiv:1203.3192)

Ouchi M. et al., 2009, ApJ, 706, 1136

Petitjean P., Bergeron J., 1990, A&A, 231, 309

Prochaska J. X., Weiner B., Chen H.-W., Mulchaey J., Cooksey K., 2011, ApJ, 740, 91

Prochter G. E., Prochaska J. X., Burles S. M., 2006, ApJ, 639, 766

Reddy N. A., Steidel C. C., 2009, ApJ, 692, 778

Rubin K. H. R., Weiner B. J., Koo D. C., Martin C. L., Prochaska J. X., Coil A. L., Newman J. A., 2010, ApJ, 719, 1503

Scoville N. et al., 2007, ApJS, 172, 1

Sembach K. R., Savage B. D., 1996, ApJ, 457, 211

Shapley A. E., Steidel C. C., Pettini M., Adelberger K. L., 2003, ApJ, 588, 65

Shapley A. E., Steidel C. C., Erb D. K., Reddy N. A., Adelberger K. L., Pettini M., Marmby P., Huang J., 2005, ApJ, 626, 698

Simcoe R. A., Sargent W. L. W., Rauch M., Becker G., 2006, ApJ, 637, 648
Steidel C. C., Kollmeier J. A., Shapley A. E., Churchill C. W., Dickinson M., Pettini M., 2002, ApJ, 570, 526

Steidel C. C., Shapley A. E., Pettini M., Adelberger K. L., Erb D. K., Reddy N. A., Hunt M. P., 2004, ApJ, 604, 534

Steidel C. C., Erb D. K., Shapley A. E., Pettini M., Reddy N., Bogosavljević M., Rudie G. C., Rakic O., 2010, ApJ, 717, 289

Tripp T. M., Lu L., Savage B. D., 1998, ApJ, 508, 200

Tumlinson J. et al., 2011, Sci, 334, 948

Weiner B. J. et al., 2009, ApJ, 692, 187

Zheng Z., Coil A. L., Zehavi I., 2007, ApJ, 667, 760

This paper has been typeset from a T_EX/L^aT_EX file prepared by the author.